A Stretched Deramping Radar Technique for High-Resolution SAR Processing in *Ka*-Band Using the Extended Integration Time

Jun Sung Park, Chul Ki Kim, and Seong Ook Park, *Senior Member, IEEE*

***Abstract*— To increase the image quality of synthetic aperture radar (SAR) is one of the hot issues for high-performance detection/reconnaissance. With this interest in the SAR technique, it generates various techniques according to the purposed platforms (Auto-SAR, ViSAR, InSAR, and PolSAR). In this article, we introduce high-efficiency and useful techniques, which can be applied to various SAR applications for generating high-quality images in the *Ka*-band. We proposed the stretched deramping hardware system applicable in the *Ka*-band, and design the Range-Doppler algorithm which well matches the proposed radar system with the modified signal parameters. Thus, we can extend the integration time of the convolution process in slow time and it leads to the improvement of the SAR image quality. To verify the performance of our proposed technique, we process the practical experiments in conventional outdoor fields. Furthermore, the proposed method is operated on the range Doppler algorithm (RDA), which is mostly used for standard SAR.**

***Index Terms*— Automobile synthetic aperture radar (Auto-SAR), extended integration time, *Ka*-band deramping radar, SAR experimental verification.**

I. Introduction

In THE 1960s, synthetic aperture radar (SAR) was only studied for military use. However, since then, SAR has been extended to a variety of applications, such as satellites, due to its ability to monitor target areas regardless of weather and time conditions. Conventional SAR research has been studied for ground observation at the *L*-/*C*-/*X*-band [1], [2], [3]. And also, large-scaled satellites have been developed for various purposes (InSAR, PolSAR, 3-D-SAR, and Spotlight-SAR) [4], [5]. Recent research shows that it is possible to study a miniaturized system with high performance due to the advanced hardware system and signal processing. It leads to manufacturing several small satellites (i.e., satellite constellation) at a lower cost than one large-scaled satellite. Furthermore, the satellite constellation can carry out real-time monitoring of the interested area and enlarge the reconnaissance coverage [6]. For this reason, it is important to study the satellite constellation for reducing the monitoring cycle time and increasing efficiency rather than one large satellite. However, it is difficult to design a small satellite in the *L*-/*C*-/*X*-band, which has a relatively long wavelength that leads to a larger size of the overall radar system [7]. Therefore, a radar system at millimeter wave (over *Ka*-band) has been suggested as a good alternative for the solution to miniaturize the hardware system [8], [9]. By employing high frequency, it can also generate a chirp signal with a wide bandwidth, which enables a high-resolution SAR image. Unfortunately, there are problems to be solved in order to use the above advantages. According to the Nyquist sampling theorem, a high sampling rate analog-to-digital converter (ADC) is required to guarantee a wide bandwidth of chirp signal in the radar system [10]. It is one of the most difficult reasons to make a high-resolution chirp pulse radar system. A high sampling rate causes high cost and generates massive data. And also, it leads to an increase in the computational amount and time. Therefore, the deramping radar structure has been recommended to reduce the minimum required sampling rate of receiver ADC by mixing the signals at the analog stage [11] without changing the resolution bit number. To a lot of researchers, the conventional deramping structures are designed with a novel hardware system with suitable signal processing techniques [29], [30], [31], [32]. Nevertheless, the deramping radar architecture, operated in a high frequency, still has some limitations to use in practice. First, the deramping structure uses the RF time-delay elements to control the mixing between Tx and Rx signals. It can increase the cost and the complexity of manufacturing and operating the radar system. Especially, a satellite radar system for long-range detection needs a time-delay component to preserve resolution. Without the time-delay technique, the deramped region between the reference and received signals decreases, which drives the low quality of the SAR image [12]. Another severe pathloss is at high frequency. As the frequency increases, the energy of the transmitted (TX) signal is rapidly decreasing due to the interference of the atmosphere [13]. In summary, a high-frequency RF time-delay element is difficult to handle accurately and it can increase the complexity of the overall radar system. And due to severe path loss at the *Ka*-band,

Manuscript received 14 December 2022; revised 21 February 2023; accepted 15 March 2023. Date of publication 3 April 2023; date of current version 13 April 2023. This work was supported in part by the Institute of Information and Communications Technology Planning and Evaluation (IITP) grant funded by the Korean Government (MSIT) (K-Drone Detection and Anti-Drone Integrated System Development) under Grant 2021-0-00908, and in part by the Institute of Information and Communications Technology Planning and Evaluation (IITP) grant funded by the Korean Government (MSIT) (Key Technologies Development for Next Generation Satellites) under Grant 2018-0-01658. The Associate Editor coordinating the review process was Dr. Yuan Gao. *(Corresponding author: Chul Ki Kim.)*

The authors are with the School of Electrical Engineering, Korea Advanced Institute of Science and Technology, Daejeon 34141, South Korea (e-mail: kirasnip@kaist.ac.kr; chulki@kaist.ac.kr; soparky@kaist.ac.kr).

Digital Object Identifier 10.1109/TIM.2023.3264048

it is hard to achieve a clear SAR image. Furthermore, direct leakage is an inevitable problem in the frequency-modulated continuous-wave (FMCW) mode, which causes RF problems in the system and degrades the signal quality [14], [15], [16]. The deramping system is operated on the scheduled time plan of each signal. However, it is conventionally suitable for medium- or long-range SAR measurement applications [17]. In addition, it is difficult to use in the case of a certain short distance. Because the time interval between the received signal and the reference signal is reduced, direct leakage inevitably occurs.

In this article, we propose an advanced deramping heterodyne radar structure and extend the integration time for azimuth-matched filter in signal processing algorithm with the stretched reference signal in *Ka*-band (over 30 GHz). The proposed platform can compensate the severe pathloss and will be easy to operate a deramping radar system without the RF time-delay components. Simultaneously, we can obtain stable performance without the degraded resolution according to the detection range. In addition, problems (phase noise, noise floor, and aliasing), mainly caused by direct leakage, are solved through the signal time schedule and frequency planning within the available system frequency bandwidth coverage. That is, we can obtain high-quality SAR images not only for mid/long range but also for short range. To generate a high-quality image at the *Ka*-band, we try to increase the Doppler bandwidth with a low sidelobe antenna. In other words, the Doppler chirp rate in the azimuth plane is proportional to the target frequency and the designed low sidelobe antenna can secure a wider integration time [18]. With the proposed antenna, we try to calculate the suitable matched filter to use the extended Doppler band. We also suggest the guideline of signal timing graph and frequency plan to achieve the desired performance. As a result, with the proposed *Ka*-band deramping system, the above phenomena lead to getting a higher signal-to-noise ratio (SNR) property of the received signal through the azimuth compression using extended integration time in signal processing. We design the baseband system block with two signal sources to implement a time delay of a conventional deramping system without a specific RF time-delay element. And also, it can be implemented by the proposed time scheduling for the deramping system without an additional RF time controller. The radar system, which is based on the RF time elements, can be operated in limited conditions, such as time delay and input frequency dynamic range, etc. Thus, in this article, we try to introduce our know-how and skills, which are useful to develop the deramping radar in the high-frequency band. Furthermore, diverse system techniques are applied to ensure stable and clear signals for transmission and reception. We can analyze and reduce the system noise to improve the total system SNR.

In order to verify the proposed technique, we manufacture the prototype of the deramping radar system at the *Ka*-band. And also, it is designed for an automobile platform (Auto-SAR) [19]. Through the practical experiment on the highway, we obtained raw data on strip-map mode and prove the performance by generating high-quality *Ka*-band auto-SAR images using the proposed system and the extended integration time in the azimuth direction.

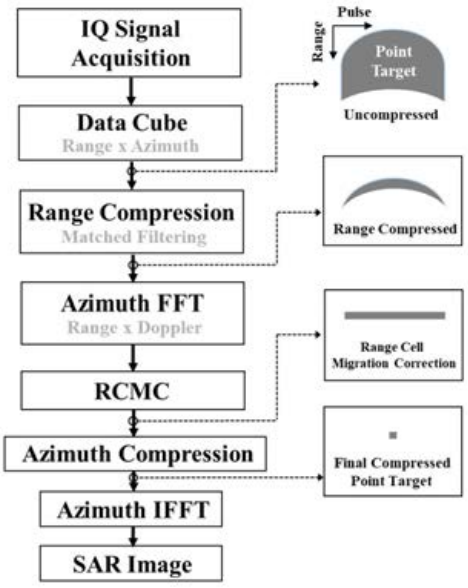

Fig. 1. Conventional RDA.

The remainder of this article is organized as follows.

Section II introduces the standard theory for generating SAR images. Section III provides our proposed hardware system and the signal processing technique "the extended integration time" at high frequency. Section IV shows the results from the practical experiment to verify the reliability and validity of our proposed scheme. Finally, in Section V, we summarize the conclusion.

II. Background Theory for Standard SAR

In order to study SAR processing, it is helpful to understand the standard modeling of signals for transmission and reception. Thus, we can analyze the conventional range-Doppler algorithm (RDA) model based on mathematical theory. And then, the final deramping signal model, which is fundamental to our proposed method, will be introduced in this section.

The RDA is one of the signal processing algorithms to obtain 2-D-SAR images, and it is analyzed for our proposed algorithm in this article [18]. The RDA compresses the raw data in range direction (fast-time) and azimuth direction (slow-time) with each matched filter, respectively. Fig. 1 introduces the RDA for the SAR process on strip-map mode. And, Fig. 2 shows the strip-map mode automobile SAR geometry in the low-squint case. The standard signal processing of RDA is composed of range and azimuth compressions and range cell migration correction (RCMC). The Doppler estimation for azimuth-matched filter should be applied to obtain high-quality images in high squint cases. Although inaccurate estimation of Doppler frequency is critical to the image quality in the case of airborne or spaceborne SAR, it is insignificant to apply the estimation method to Auto-SAR, which is in low-squint (zero-Doppler centroid) [20]. For the analysis of the RDA process,

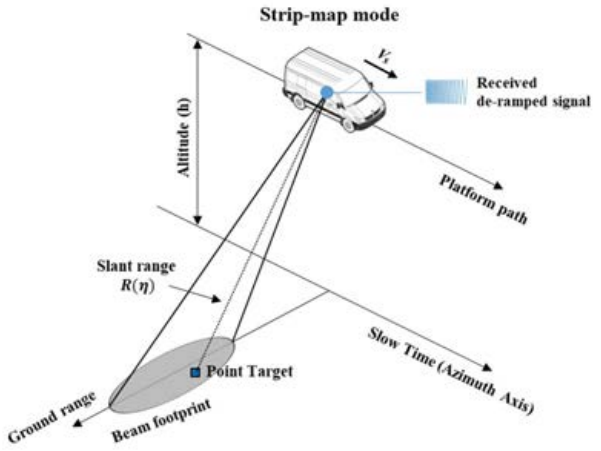

Fig. 2. Strip-map mode automobile SAR geometry in the low-squint case.

the received demodulated I/Q signal for the low squint case can be defined as follows [18]:

$$S_{\text{received}}(\tau,\eta) = A_r\omega_r\left[\tau-\frac{2R(\eta)}{c}\right]\omega_a[\eta-\eta_c]e^{-j\frac{4\pi f_0 R_0}{c}} \times e^{j\pi K_r\left[\tau-\frac{2R(\eta)}{c}\right]^2}e^{-j\frac{2\pi f_0 V_r^2\eta^2}{cR_0}} \quad (1)$$

where τ and η are the range and azimuth time, respectively, ω_r is the window function of range direction, ω_a is a two-way antenna beam pattern in the azimuth direction, A_r is the amplitude of the signal, η_c is the Doppler centroid azimuth time, f_0 is the center frequency of the chirp pulse signal, R_0 is the target slant range at the closest approach, c is the speed of light, V_r is the nominal platform speed, K_r is the range direction chirp rate of the signal, and $R(\eta)$ is the instantaneous slant range. The range-matched filter, generated by the system parameters (chirp bandwidth and chirp duration), and the signal model in (1) are processed by convolution [21]. And the fast Fourier transform (FFT) is performed in the azimuth direction to make a range-Doppler map. After that, the range bin of each target is corrected through the RCMC process. Likewise, the azimuth-matched filter, designed with the Doppler parameter, is used to compress the signal in the azimuth direction. From the matched filtering in range and azimuth direction, the following equation can be derived with inverse FFT [18]

$$S_{ac}(\tau,\eta) = A_o p_r\left[\tau-\frac{2R_0}{c}\right]p_a[\eta]e^{-j\frac{4\pi f_0 R_0}{c}}e^{j2\pi f_{\eta_c}\eta} \quad (2)$$

where p_r and p_a are the sinc-like function, f_{η_c} is the Doppler centroid frequency, and A_o is the amplitude. The point target is compressed at $\tau = (2R_0/c)$ and $\eta = 0$. In RDA for the processing, model called deramping or otherwise called FMCW, the range compression can be replaced by the physical processing of the hardware system [12]. The beat signals of each target are generated by mixing the reference signal and the received signal. The final received raw data at an intermediate frequency, including beat signals, is shown as follows:

$$S_{\text{IF}}(\tau,\eta) = A_{\text{IF}}\omega_{\text{overlap}}[\tau]\omega_a[\eta-\eta_c] \times \cos\left[2\pi f_{\text{IF}}\tau-\frac{4\pi K_r R(\eta)}{c}\tau-\frac{4\pi f_0 R(\eta)}{c} +\pi K_r\left(\frac{2R(\eta)}{c}\right)^2\right] \quad (3)$$

where ω_{overlap} is the window function which represents the overlap region of TX signal replica and received signal, f_{IF} is the intermediate frequency, and A_{IF} is the amplitude. The beat signal can be extracted from the second phase term of (3). In the chirp pulse model, the information of range can be expressed in the time domain. While, in the deramping model, we can obtain the beat frequency, which indicates range information, using FFT as follows:

$$S_{\text{IQ\_FFT}}(f_\tau,\eta) = A_r P_r\left[f_\tau - f_{\text{beat}}\right]\omega_a[\eta-\eta_c] \times e^{j\left(\pi K_r\left(\frac{2R(\eta)}{c}\right)^2-\frac{4\pi f_0 R(\eta)}{c}\right)} \quad (4)$$

where P_r is the sinc-like envelope function in the frequency domain, and f_{beat} is the beat frequency of the point target. Moreover, the minimum required ADC sampling rate is defined by the bandwidth of the received signal, and the bandwidth of the beat frequency is lower than the bandwidth of the TX signal. Hence, the FMCW model can reduce the sampling rate than the chirp pulse system to detect a wide swath range while maintaining high resolution. Although the deramping model can secure a wide bandwidth, it still has the disadvantage of decreasing the resolution along the detection range.

TABLE I
SUMMARY OF PROPERTY OF CHIRP PULSE AND FMCW RADAR SYSTEM

Radar Type	Required Sampling Rate	Direct Leakage	Bandwidth Limitation (fixed ADC)	Peak Power
Chirp Pulse	High	Low	High	High
FMCW	Low	High	Low	Low

The advanced delay-stretched de-ramping structure, we use in this article, gathers the advantages of both radar systems (chirp pulse and FMCW radar). Table I introduces a summary of each radar system with its pros and cons. The advanced deramping radar system transmits the signals as chirp pulse radar and receives them as FMCW radar. In other words, the proposed radar system transmits the pulse signal, which has the advantage of increasing the maximum detectable range. Simultaneously, the proposed radar receives the deramped signal, which is the beat frequency. It can reduce the sampling rate of raw data and the complexity of signal processing. The final signal model, processed by the deramped algorithm, can be expressed with beat frequency and azimuth compressed signal, shown as

$$S_{\text{final}}(f_\tau,\eta) \approx A_o P_r\left[f_\tau - f_{\text{beat}}\right]p_a[\eta]e^{-j\frac{4\pi f_0 R_0}{c}}e^{j2\pi f_{\eta_c}\eta}. \quad (5)$$

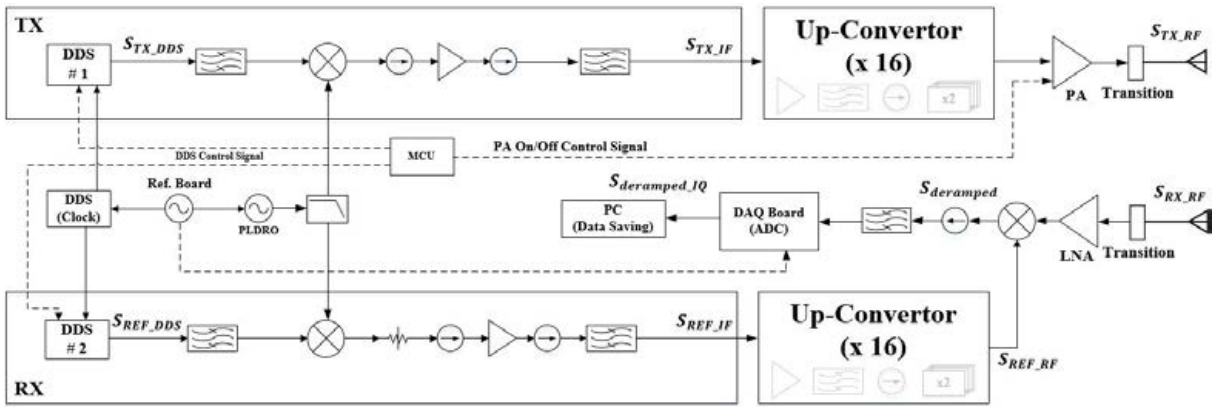

Fig. 3. Block diagram of the proposed *Ka*-band delay-stretched deramping radar system.

To demonstrate our proposed technique, we will explain the overall technique in the next two sections (hardware system and signal processing). In Section III-A, the radar architecture is designed for deramping mode with a stretched reference signal. In Section III-B, we analyze and propose the RDA, which is well-matched with the proposed deramping system, from the perspective of signal processing.

III. Proposed SAR Technique Through Deramping System and Signal Process

A. Proposed Ka-Band Delay-Stretched Deramping Heterodyne Radar Structure

The deramping system combines the advantages of chirp pulse and FMCW radar. High transmission power, which is the property of chirp pulse radar, can be used, and sampling rate and raw-data size can be reduced as FMCW radar. Therefore, to propose a SAR system, based on de-ramping radar, we design the delay-stretched deramping heterodyne radar system at the *Ka*-band, as shown in Fig. 3. In this section, we propose how to design the hardware system and support various considerations for the proposed deramping SAR system at the *Ka*-band. With the proposed hardware system, it enables the achievement of a full Doppler band at the whole interesting range without resolution loss. In our case, in order to utilize the wide-stretched reference signal, wide system bandwidth is designed for operating the proposed deramping radar. We scheme a structure using four frequency doublers to obtain high frequency and wide system bandwidth with high linearity. Each baseband signal is up-converted to a 2-GHz signal and multiplied up to *Ka*-band by four frequency doublers. In addition, various bandpass filters are used to suppress spurs from nonlinearity elements. Conventionally, this structure amplifies the quantization error of the final *Ka*-band linear chirp signal [22]. To prevent this phenomenon, we used a high clock direct digital synthesizer (DDS) to minimize the step size of frequency and time at the baseband signal. In the SAR application, without the time-delay parameter, the overlapped region between the round-trip and TX replica signal will be decreased along with the distance. The time delay of the TX signal replica is essential to preserve the resolution of the SAR image because the decrease of the overlapped region leads to a reduction of the resolution of the SAR image [12]. However, the high-frequency RF time delay elements are difficult to handle accurately and increase the operational complexity of the overall radar system. Therefore, we propose our delay-stretched structure that can achieve the equivalent effect of RF time delay elements. Two DDSs are applied to the delay-stretched system to manage the time schedule for the baseband signals. Each DDS is assigned for the TX signal and reference signal in each baseband part, respectively. The microcontroller, called ATMEGA 128, is worked in 62.5-ns time control resolution for operating two DDS. With only one controller, we can easily handle diverse parameters of TX/reference chirp signals in the digital domain. The controlled parameters are constructed as chirp bandwidth, chirp duration, center frequency, time/frequency step, and each starting time of two DDSs. The proposed radar system is synchronized by one reference clock, which is "'10 MHz." And also, synchronization pins at two signal sources are bridged into each control block. It ensures the whole system coherence in terms of accurate signal timing. Moreover, to mix two signals for deramping, it is also necessary to match the phase coherency of baseband signals in two DDS boards. From the microcontroller, a phase correction signal is employed to process accurate azimuth-matched filtering. It leads to helpful handling to plan the schedule of signal sources for mixing Rx and reference signals according to target range coverage. In order to extract high-quality image in high-frequency radar, a low-noise receiver should be used due to severe pathloss. Hence, we analyze and design the system to reduce prominent system noises. The dominant system noises in radar systems can be defined as quantization noise and thermal noise. Quantization noise floor level (QNFL) can be defined as follows:

$$\mathrm{QNFL} = 10\log_{10}\left(\frac{(\mathrm{FS})^2}{2\times 50}\times 1000\right) - (6.02\times N + 1.76) - 10\log_{10}(M) \quad (6)$$

where FS is the power dynamic range of ADC, N is the resolution bit number of ADC, and M is the sample number of the sampled raw data. According to (6), there are three variables that control QNFL. FS should be designed in a

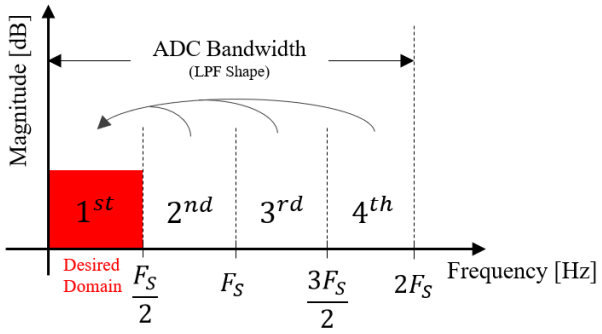

Fig. 4. Noise folding phenomenon.

direction to avoid saturation problems rather than noise, so it is desirable to set it considering OP1dB. Regardless of the type of radar, such as chirp pulse, FMCW, and deramping radar, a higher resolution bit number can generate a lower value of QNFL. Therefore, we try to use an ADC with a sufficiently high-resolution bit number. Even using the high bit number to improve the SNR (low noise), the proposed deramping structure can support the low sampling rate to reduce the data size. Conventionally, for detecting the target, it is important to design a low-noise radar system. Simultaneously, in our designed radar system, we try to focus on developing the stretched deramping technique to reduce the sampling rate. From this concept, Universal Software Radio Peripheral (USRP) N210 board and additional daughter board WBX-40 are used, which has 20-MHz bandwidth and 16-resolution bit number to get I/Q raw data. Moreover, the thermal noise floor level (TNFL) can be defined as follows:

$$\text{TNFL} = -174 + 10\log_{10}(\text{Analog BW}) - 10\log_{10}(M) + G_r + \text{NF} \quad (7)$$

where Analog BW is the analog pass-bandwidth, G_r is the receiver gain, and NF is the noise figure. We try to minimize the signal power loss between the RX antenna and LNA by using a short, low-loss cable to achieve a low noise figure in the system [23]. In addition, in the case that the analog bandwidth of ADC is wider than the desired digital bandwidth, the noise outside of the Nyquist zone is folded into the desired domain, as shown in Fig. 4 [24]. A bandpass filter suitable for the predetermined digital bandwidth is used in front of the data acquisition (DAQ) board to prevent the noise folding phenomenon. And also, we select a higher sampling rate than the minimum required sampling rate, called oversampling, to secure high SNR [25], [26]. Therefore, in summary of the proposed signal flow in the system, two DDSs generate each baseband signal with the time gap. Each signal is modulated for IF signals and these IF signals are 16 times multiplied by four frequency-doublers. Finally, the TX signal is reflected by the target and is deramped with the delay-stretched reference signal to make a beat signal. In the next step, the RDA signal processing model with the extended integration time is described in detail. Furthermore, we show the results to verify the whole proposed SAR technique in Section IV.

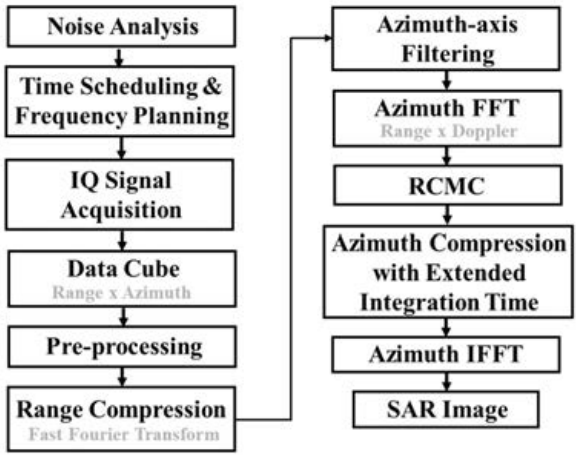

Fig. 5. Proposed RDA for delay-stretched deramping SAR.

B. Proposed SAR Signal Processing Design With Extended Integration Time

To manage the deramped I/Q raw data, we choose the RD algorithm, mostly used for SAR signal processing. Furthermore, we design the azimuth-matched filter for the extended integration time with the RD algorithm. It can improve the quality of SAR images at the high-frequency band. Unlike chirp pulse SAR, the focused SAR image is generated in the frequency domain along the range direction by FFT. Fig. 5 shows the overall process of our proposed algorithm with time scheduling and frequency planning. There are five steps to obtain a high-quality SAR.

1) *Time Scheduling and Frequency Planning:* Schedule the time and frequency of the signal for the deramping technique
2) *Preprocessing:* Raw data arrangement and process to improve the signal quality.
3) *FFT in Range Direction:* Focusing the targets of the SAR image along the range direction.
4) *RCMC:* Correcting the quadratic term of range cell migration (RCM) factor to match the azimuth-matched filter
5) *Azimuth Compression:* Compressing the targets in the azimuth direction using the matched filter with the extended integration time

To understand our deramping radar system, we analyze the time scheduling and frequency planning with the TX and reference signals. It is useful to implement the deramping hardware system without additional RF time delay elements. We need to arrange the raw data while reducing the interference of disturbing signals. After 3), FFT in range direction (range compression), the process of generating a deramped SAR image will be described in 4) RCMC and 5) Azimuth Compression. Based on the proposed hardware system, step 5) is the additional procedure to extend the azimuth time in the matched filter for the high-quality deramped SAR image.

As mentioned above, it is important to apply accurate signal processing to the proposed delay-stretched deramping model. The overall frequency planning with the intermediate

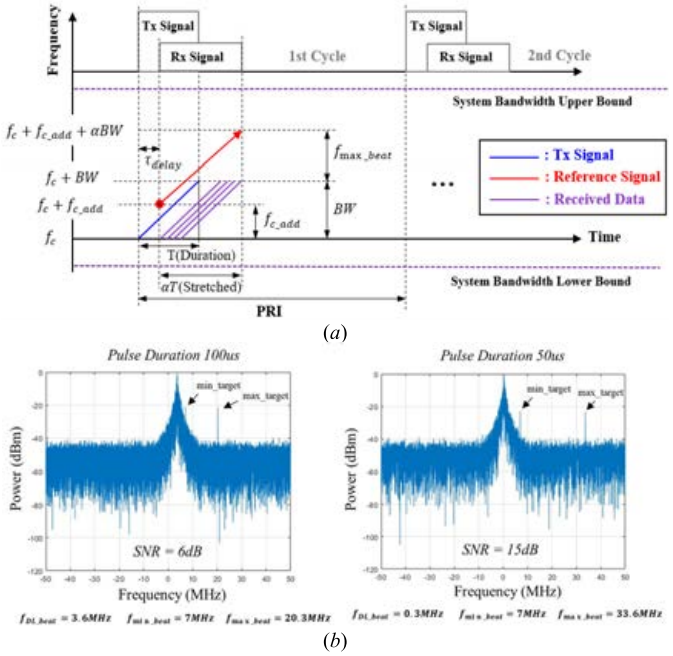

Fig. 6. (a) Frequency planning and signal time graph of TX/REF signal. (b) Expected target signals in the beat frequency domain.

frequency must be defined to take advantage of our proposed deramping mode. And also, the signal timing graph is accurately scheduled to apply the time-shifting and stretching techniques. As shown in Fig. 6(a), we show the frequency planning and signal time graph. As explained in the previous section, we consider the time/frequency values of the TX and reference signals according to the required conditions (minimum/maximum detection range and resolution) within the system frequency bandwidth. And also, sufficient spacing between direct leakage and received data should be ensured by setting our proposed parameters. As shown in Fig. 6(b), we can detect the expected target points with decreased noise floor. It leads to alleviating the rise of noise floor due to the phase noise of the direct leakage signal [14]. The beat signal by the direct leakage and the target can be induced as follows:

$$\begin{aligned} f_{\mathrm{DL\_beat}} &= f_{c\_\mathrm{add}} - 16K_r\tau_{\mathrm{delay}} \\ f_{\mathrm{min\_beat}} &= f_{c\_\mathrm{add}} - 16K_r\tau_{\mathrm{delay}} + \frac{32K_r}{c}R_{\mathrm{min}} \\ f_{\mathrm{max\_beat}} &= f_{c\_\mathrm{add}} - 16K_r\tau_{\mathrm{delay}} + \frac{32K_r}{c}R_{\mathrm{max}} \end{aligned} \tag{8}$$

where f_{c_add} is the frequency gap between the TX signal and the reference signal, τ_{delay} is the time delay of the reference signal for deramping, R_{min} is the minimum interested range, and R_{max} is the maximum interested range. From the above equations, the beat frequencies are proportional to the maximum/minimum interested range and can be variably controlled, based on the chirp rate, time delay, and additional carrier frequency. By controlling the chirp rate and time interval between the TX signal and the reference signal, the interference of direct leakage is rapidly reduced within the interested data. Conventionally, deramping structures do not exist the problem from direct leakage, but it is only for mid-/long-range radar. Through the above frequency planning and time schedule, the advantages of deramping can be achieved not only at mid-/long-range radar but also at certain short-range radar. It means that, even in the short-range mode, we can handle the expected target range by reducing the interference of direct leakage as shown in Fig. 6(b).

TABLE II
CONSIDERABLE SYSTEM PARAMETERS

	Control Variable	Limitation
Interested Range	Time Delay, *Stretch Factor	Sampling Rate (ADC)
Resolution	Chirp Bandwidth	System Frequency Bandwidth
Separation (between Direct Leakage and Received Signal)	Chirp Duration (Chirp Rate)	Sampling Rate, (ADC) Maximum Detectable Range
Chirp Duration	-	Duty Cycle, (Power Amplifier) Frequency Bandwidth (Radar System)

*: The parameters of reference signal (chirp rate, delay time, center frequency, etc.)

The stretching technique presents that the reference signal, matched with the TX signal, is stretched in the coverage of the system usable bandwidth. The stretched reference signal is deramped (mixed) with the reflected signal by the target. Depending on the interested range, the stretched length and delay time of the reference signal can be determined. As shown in Fig. 6(a), all received signals can be deramped by full bandwidth with a reference signal (stretched signal). It means that we can obtain an SAR image without the decreased resolution along all range coverage. Table II shows the summary of the controlled parameters and limited conditions for signal time scheduling and frequency planning.

To analyze the proposed signal model, we start to introduce the analytic signals at each DDS. For simplicity of explanation, the amplitude values of chirp signals are unified in one parameter (A_n). And also, due to variable time scaling, the window function is defined as follows:

$$\omega_{rs}[\tau] = \begin{cases} 1, & \text{when } 0 < \tau < T \\ 0, & \text{otherwise.} \end{cases} \tag{9}$$

The baseband signals from two DDSs can be expressed as follows:

$$S_{\mathrm{TX\_Analytic}}(\tau) = A_1\omega_{rs}[\tau]e^{j\pi K_r\tau^2} \tag{10}$$

$$S_{\mathrm{TX_{DDS}}}(\tau) = A_2\omega_{rs}[\tau]\cos\left[2\pi f_{\mathrm{IF\_TX}}\tau + \pi K_r\tau^2\right] \tag{11}$$

$$S_{\mathrm{REF_{Analytic}}}(\tau) = A_3\omega_{rs}\left[\frac{\tau-\tau_{\mathrm{delay}}}{\alpha}\right]e^{j\pi K_r(\tau-\tau_{\mathrm{delay}})^2} \tag{12}$$

$$\begin{aligned} S_{\mathrm{REF\_DDS}}(\tau) = A_4\omega_{rs}&\left[\frac{\tau-\tau_{\mathrm{delay}}}{\alpha}\right] \\ &\times\cos\left[2\pi f_{\mathrm{IF\_REF}}(\tau-\tau_{\mathrm{delay}})+\pi K_r(\tau-\tau_{\mathrm{delay}})^2\right] \end{aligned} \tag{13}$$

where ω_{rs} is the shifted rectangular window function, A_n is the amplitude factor, $f_{\mathrm{IF\_TX}}$ and $f_{\mathrm{IF\_REF}}$ are the IF frequency of each DDS output signal, and α is the stretch factor. Especially, τ_{delay} and α are determined by the interested range. Note that α controls the stretched value of the reference signal with the fixed chirp rate. And also, K_r is adjusted to increase the gap from direct leakage within the system bandwidth. The signal generated by DDS is up-converted and multiplied by four frequency doublers. RF signals can be expressed as

$$S_{\mathrm{TX\_RF}}(\tau) = A_5\omega_{rs}[\tau]\cos\left[2\pi f_c\tau + \pi 16K_r\tau^2\right] \tag{14}$$

$$S_{\mathrm{REF_{RF}}}(\tau) = A_6\omega_{rs}\left[\frac{\tau-\tau_{\mathrm{delay}}}{\alpha}\right] \times \cos\left[2\pi\left(f_c + f_{c_{\mathrm{add}}}\right)\left(\tau-\tau_{\mathrm{delay}}\right) + \pi 16K_r(\tau-\tau_{\mathrm{delay}})^2\right] \tag{15}$$

where f_c indicates the carrier frequency. Note that the chirp rate is 16 times from the above baseband signal. In our case, although the proposed structure with four frequency doublers has the advantages of obtaining high frequency and wide system bandwidth, it can increase the quantization error during frequency modulation. To overcome this problem, we minimize the frequency/time step of the baseband linear frequency modulation (LFM) signal by operating the DDS with a high-rate reference clock. The received signal from the stationary point target is expressed as follows:

$$\tau_{r.t} = \frac{2R(\eta)}{c} \tag{16}$$

$$S_{\mathrm{RX\_RF}}(\tau,\eta) = A_7\omega_{rs}[\tau-\tau_{r.t}]\omega_a[\eta-\eta_c] \times \cos\left[2\pi f_c(\tau-\tau_{r.t}) + \pi 16K_r(\tau-\tau_{r.t})^2\right] \tag{17}$$

where $\tau_{r.t}$ is the round-trip time. The received signal in (17) is deramped (mixed) with the delay-stretched reference signal, as shown in (15). It leads to the beat signal, which means the range information of the SAR

$$S_{\mathrm{Deramped}}(\tau,\eta) = A_8\omega_{\mathrm{overlap}}[\tau]\omega_a[\eta-\eta_c] \times \cos\left[\left(2\pi f_{c\_\mathrm{add}} - 32\pi K_r\tau_{\mathrm{delay}} + 32\pi K_r\tau_{r.t}\right)\tau + 2\pi f_c\tau_{r.t} - 16\pi K_r\tau_{r.t}^2 + \theta_s\right] \tag{18}$$

where $\theta_s = 16\pi K_r\tau_{\mathrm{delay}}^2 - 2\pi f_c\tau_{\mathrm{delay}} - 2\pi f_{c\_\mathrm{add}}\tau_{\mathrm{delay}}$.

This scheme is the same as that of the range compression in the chirp pulse radar system. The deramped beat signal is sampled and I/Q demodulated by USRP N210. The sampled I/Q raw data can be expressed as follows:

* Proposed final de-ramped IQ signal

$$S_{\mathrm{Deramped\_IQ}}(\tau,\eta) \approx A_9\omega_{\mathrm{overlap}}[\tau]\omega_a[\eta-\eta_c] \times e^{j\left(\left(-32\pi K_r\tau_{\mathrm{delay}}+32\pi K_r\tau_{r.t}\right)\tau + \frac{4\pi f_c R_0}{c} + \frac{2\pi V_r^2}{\lambda R_0}\eta^2 + \theta_s\right)}. \tag{19}$$

After FFT along the range direction, to remove the ghost target, filtering is performed in the azimuth direction. Sufficient PRF must be ensured. Before the RCMC and compression process, the raw data are converted into the range(beat)-Doppler domain through FFT in the azimuth direction. A series of target trajectories in the same range are converted into one single trajectory. The raw data in the range(beat)-Doppler domain are expressed as follows:

$$S_{rD}(f_\tau, f_\eta) = A_{10}P_r\left[f_\tau - f_{\mathrm{beat}}\right]W_a\left[f_\eta - f_{\eta_c}\right] \times e^{j\left(\frac{4\pi f_c R_0}{c}+\theta_s\right)}e^{-j\pi\frac{f_\eta^2}{K_{\mathrm{az}}}} \tag{20}$$

where K_{az} is the azimuth FM rate. The principle of stationary phase (POSP) is used for derivation [27]. And the slant range equation on the range-azimuth domain and range-Doppler domain can be expressed in the low squint case as follows:

$$R(\eta) = R_0 + \frac{V_r^2\eta^2}{2R_0}$$

$$R_{\mathrm{rd}}(f_\eta) = R_0 + \frac{R_0\lambda^2}{8V_r^2}f_\eta^2 \tag{21}$$

where V_r is the SAR platform velocity. Although the quadratic RCM term can be compensated, we are able to focus on various targets of SAR images without the RCMC in high-frequency and short-range radar [20]. After RCMC, an azimuth-matched filter is applied to compress the spread

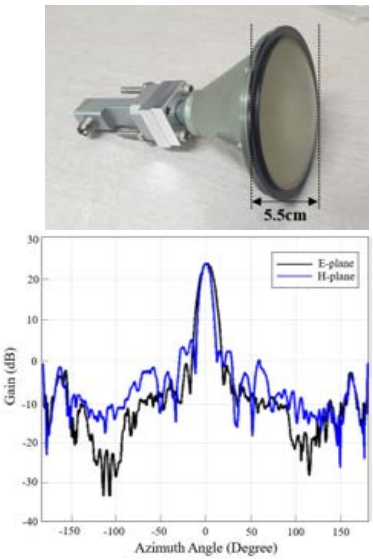

Fig. 7. Antenna specification.

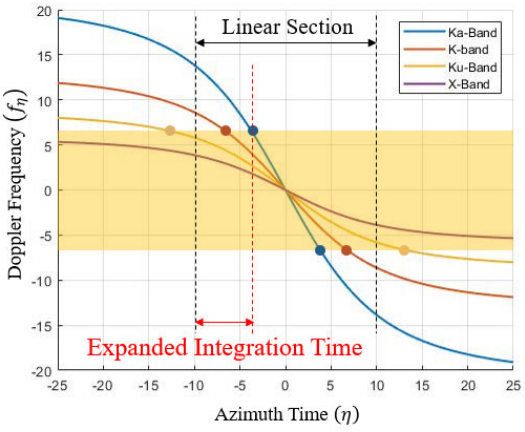

Fig. 8. Doppler frequency map according to the frequency.

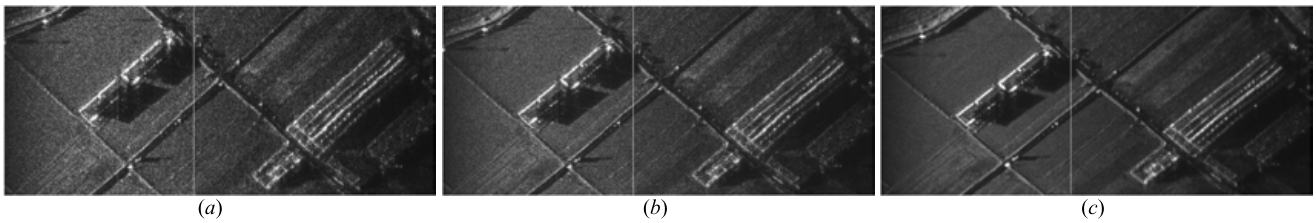

(a) (b) (c)

Fig. 9. SAR image variation at the *Ka*-band according to the integration time. (a) Insufficient time (0.1 s). (b) Conventional time (0.5 s). (c) Extended time (0.8 s).

Fig. 10. Measurement setup for automobile-SAR.

target data into a point target. Based on the above-expected signals and the characteristics of high frequency, we can design the matched filter with the extended exposure time to improve the focusing quality of targets. In general, the exposure time and frequency modulated rate in the azimuth direction are derived as follows, respectively [18]:

$$T_a = 0.886\frac{R(\eta_c)\lambda}{L_a V_g \cos\theta_{r,c}}$$
$$K_{\text{az}} = \frac{2}{\lambda}\frac{d^2R(\eta)}{d\eta^2}\bigg|_{\eta=\eta_c} = \frac{2V_r^2\cos^2\theta_{r,c}}{R(\eta_c)\lambda} \tag{22}$$

where L_a is the antenna length in the azimuth direction, $\theta_{r,c}$ is the squint angle. Related to the antenna beam pattern, with a low sidelobe level, we can secure the extended Doppler band and it leads to increasing the quality of the SAR image. The designed antenna in Fig. 7 has a low sidelobe level, which reduces the unexpected interference, and it leads to receiving a clear Doppler signal, which can also increase SNR [28]. As shown in Fig. 8, more integration time is required at a lower frequency to secure the same size of the Doppler band. In other words, we can increase the Doppler frequency band at the higher frequency, using the same integration time. Therefore, it is important to utilize the expected full Doppler band, which is over 3-dB beamwidth of the designed antenna, which has low sidelobe level. It causes the increased integration time in azimuth-matched filtering. Therefore, the extended integration time, by the characteristics of the high-frequency model and the designed antenna, can improve the quality of the 2-D SAR image. Considering the above phenomenon, we design the azimuth-matched filter

$$\omega_{\text{az}}[\eta] = \begin{cases} 1, & \text{when} -\dfrac{T_{\text{extended}}}{2} < \eta < \dfrac{T_{\text{extended}}}{2} \\ 0, & \text{otherwise} \end{cases}$$
$$h_{\text{az}}(\eta) = \omega_{\text{az}}[\eta]e^{-j\pi K_{\text{az}}\eta^2}. \tag{23}$$

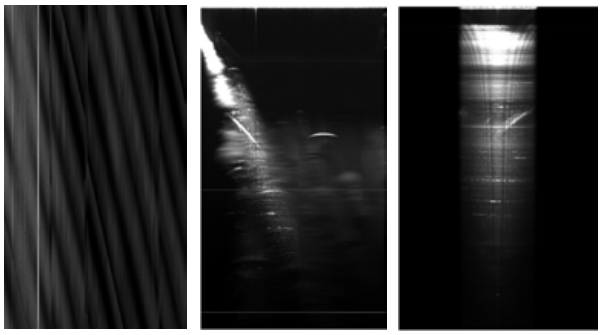

Fig. 11. Raw data, range compression, and RCMC.

The proposed azimuth-matched filter with wide integration time is designed by the above-introduced equation. In other words, based on the characteristics of the proposed *Ka*-band de-ramping radar system, we can extend the integration time of the azimuth-matched filter to the theoretically expected time. In Section IV, we will explain the processed results in more detail in Fig. 9. For achieving the high-quality SAR image, we design the overall high frequency deramping process with not only the hardware system but also the characteristic of signal processing. Finally, after finishing the above five steps, we can generate a high-quality SAR image. In Section IV, we show the method to generate a high-quality SAR image in a deramping radar system and verify our method with practical experimental data.

IV. Experiment and Results

In order to verify the proposed techniques, we manufacture a *Ka*-band deramping radar system, which is operated over 30 GHz. The system is introduced in Fig. 3, and it is used for the practical experiment. SAR in *Ka*-band has been researched to minimize and simplify the radar system, comparing *L*-/*C*-/*X*-band. It can be utilized for small satellite and

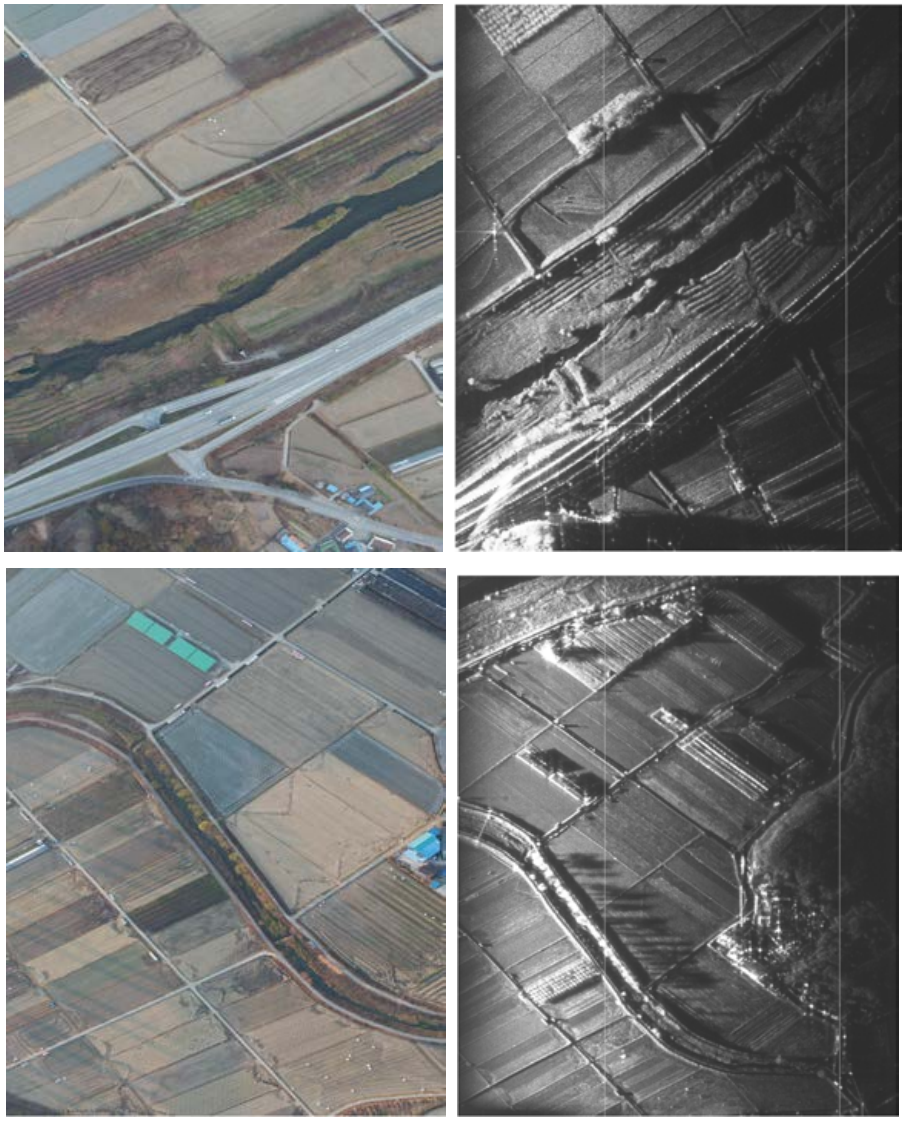

Fig. 12. Final SAR image at the *Ka*-band.

TABLE III
Ka-BAND SAR SYSTEM SPECIFICATION

Parameters	Values
Center Frequency	35.75 GHz (Ka-Band)
Bandwidth	500 MHz
Chirp Duration	200 us
LFM Waveform	Sawtooth
Transmit Power	1W(30dBm)
Sampling Frequency	< 20MHz
Oversampling Ratio	< 2.0
Platform Velocity	80km/h
Interested Swath Range	150 ~ 650m

unmanned aerial vehicles. We carried out SAR experiments on an automobile platform, called Auto-SAR, to observe the general rural topography. Table III shows the specification of the deramping radar system for the *Ka*-band.

For comparison with the conventional SAR experiment, we apply the stop-and-go method, which is used for approximate range-Doppler calculation in RDA. And also, we obtained the raw data in strip-map mode. As shown in Fig. 10, two channels are used for the operating system. The antenna closest to the front of the vehicle is connected to the channel for transmission, and the other antenna closest to the rear is connected to the channel for the reception. Fig. 7 introduces the specific design and far-field pattern of the antenna, which is also used in this SAR experiment. To secure the wide integration time, it is designed with a low sidelobe level and high gain (23 dB) at 35.75 GHz. Based on the above experimental conditions, we succeed in proving our proposed methods: 1) hardware system and 2) signal processing of the extended integration time. Fig. 11 shows the images of each step in the proposed signal processing algorithm. According to Fig. 11, from the received raw data, we can generate the compressed range image through FFT. After processing the RCMC, the final SAR images are generated with wide integrated matched filtering along the azimuth direction. Through our proposed techniques, Fig. 12 shows that the final SAR images are accurately processed in the *Ka*-band. In addition,

TABLE IV
PERFORMANCE COMPARISON FOR SAR

	Doppler Bandwidth	Hardware Weight/Volume	Image Quality
The Previous Technique [11]	Normal	Bulky	Standard (at Ku-band)
The Proposed Technique	Extended	Compact	High (at Ka-band)

Fig. 9 shows how much improvement in the image quality can be expected by increasing the integration time. Fig. 9(b) shows the SAR image, applied in conventional integration time, which is calculated with 3 dB antenna beamwidth. However, the proposed characteristics of high-frequency and low sidelobe levels in the deramping system lead to the difference in the SAR image quality. As shown in Fig. 9(c), we can confirm the quality improvement by increasing the integration time. In Table IV, we show the comparison of performance between the previous and proposed technique. We can use the extended Doppler band and reduce the hardware size of the overall system due to the utilized frequency area. Moreover, even though the proposed technique is operated at a higher frequency, it can obtain high-quality SAR images.

V. CONCLUSION

We introduce an advanced method to generate high-quality SAR image in *Ka*-band using the proposed deramping radar system and signal processing techniques of the extended integration time. With the frequency planning and time scheduling of signals, we can design the deramped SAR system and reliably generate the high-quality 2-D SAR image through the wide integration time. In other words, this article introduces the overall process of designing the deramping radar system at *Ka*-band and studies to overcome the theoretical integration time of conventional SAR processing. The effect of speckle noise is reduced according to the length of the integration section. And also, the resolution is improved due to the increased Doppler bandwidth. In this process, we can obtain a high-quality SAR image without the additional type of device to operate a deramping radar system. It means that the beat signal can be generated by the schedule of RF baseband sources without RF time delay elements and even without the degraded resolution according to the range. It leads to the low complexity of radar operation and it is easy to manipulate parameters within system conditions. Moreover, based on the proposed deramping system, we try to improve the performance by grafting the characteristics of the high-frequency signal at *Ka*-band. It can allow reducing the economic cost and the volume/weight of the overall hardware system. In Section IV, we introduce the specific explanation of a practical experiment on an actual general highway. And also, we success to verify the expected results of our proposed technique. In the end, by our proposed method, 2-D image of SAR can be generated by not only decreasing noise interference but also increasing the image quality. In line with the global trend of miniaturized satellites (CubeSat and MicroSat) at high-frequency, this article suggests the possibility of developing a radar system at the *Ka*-band. In future research, we plan to develop a novel signal processing algorithm for the airborne platform and multi-channel SAR (In-SAR and Pol-SAR). The proposed deramping radar system with extended integration time, proposed in this article, could support other SAR platforms and various applications with powerful synergy to improve the SAR image quality.

REFERENCES

[1] T. Kobayashi, S. Kojima, J. Uemoto, A. Nadai, M. Satake, and T. Matsuoka, "Observation of the eastern great earthquake disaster with the airborne SAR system (Pi-SAR2) of NICT," in *Proc. IEEE Int. Geosci. Remote Sens. Symp. (IGARSS)*, Jul. 2019, pp. 4758–4761, doi: 10.1109/IGARSS.2019.8898558.

[2] C.-S. Yang, Y.-S. Kim, K. Ouchi, and J.-H. Na, "Comparison with real SAR images and simulation SAR images of spilled oil on sea surface," in *Proc. IEEE Int. Geosci. Remote Sens. Symp.*, Jul. 2009, pp. IV-673–IV-676, doi: 10.1109/IGARSS.2009.5417466.

[3] C. K. Kim, M. T. Azim, A. K. Singh, and S.-O. Park, "Doppler shifting technique for generating multi-frames of video SAR via sub-aperture signal processing," *IEEE Trans. Signal Process.*, vol. 68, pp. 3990–4001, 2020, doi: 10.1109/TSP.2020.3006749.

[4] W. Pitz and D. Miller, "The TerraSAR-X satellite," *IEEE Trans. Geosci. Remote Sens.*, vol. 48, no. 2, pp. 615–622, Feb. 2010, doi: 10.1109/TGRS.2009.2037432.

[5] M. Zink et al., "TanDEM-X: A single-pass SAR interferometer for global DEM generation and demonstration of new SAR techniques," in *Proc. IEEE Int. Geosci. Remote Sens. Symp. (IGARSS)*, Jul. 2015, pp. 2888–2891, doi: 10.1109/IGARSS.2015.7326418.

[6] S. Marcuccio, S. Ullo, M. Carminati, and O. Kanoun, "Smaller satellites, larger constellations: Trends and design issues for Earth observation systems," *IEEE Aerosp. Electron. Syst. Mag.*, vol. 34, no. 10, pp. 50–59, Oct. 2019, doi: 10.1109/MAES.2019.2928612.

[7] C. A. Balanis, *Advanced Engineering Electromagnetics*, 2nd ed. Hoboken, NJ, USA: Wiley, 2012.

[8] M. Mcnicholas, J. Deluna, R. Manno, and Y.-H. Shu, "Low cost Ka-band transmitter for CubeSat systems," in *Proc. Top. Workshop Internet Space (TWIOS)*, Jan. 2017, pp. 1–4, doi: 10.1109/TWIOS.2017.7869770.

[9] A. Cuttin et al., "A Ka-band transceiver for CubeSat satellites: Feasibility study and prototype development," in *Proc. 48th Eur. Microw. Conf. (EuMC)*, Sep. 2018, pp. 930–933, doi: 10.23919/EuMC.2018.8541695.

[10] A. V. Oppenheim and R. W. Schafer, *Discrete-Time Signal Processing*, 3rd ed. London, U.K.: Pearson, 2010.

[11] D.-H. Jung, D.-H. Kim, M. T. Azim, J. Park, and S.-O. Park, "A novel signal processing technique for Ku-band automobile FMCW fully polarimetric SAR system using triangular LFM," *IEEE Trans. Instrum. Meas.*, vol. 70, 2021, 8500210, doi: 10.1109/TIM.2020.3011601.

[12] M. Jankiraman, *FMCW Radar Design*. Norwood, MA, USA: Artech House, 2018.

[13] H. T. Friis, "A note on a simple transmission formula," *Proc. IRE*, vol. 34, no. 5, pp. 254–256, May 1946, doi: 10.1109/JRPROC.1946.234568.

[14] J. Park, S. Park, D.-H. Kim, and S.-O. Park, "Leakage mitigation in heterodyne FMCW radar for small drone detection with stationary point concentration technique," *IEEE Trans. Microw. Theory Techn.*, vol. 67, no. 3, pp. 1221–1232, Mar. 2019.

[15] J. Park, D. Jung, K. Bae, and S. Park, "Range-Doppler map improvement in FMCW radar for small moving drone detection using the stationary point concentration technique," *IEEE Trans. Microw. Theory Techn.*, vol. 68, no. 5, pp. 1858–1871, May 2020.

[16] J. Park, J.-S. Park, K.-B. Bae, and S.-O. Park, "Advanced stationary point concentration technique for leakage mitigation and small drone detection with FMCW radar," *IEEE Trans. Microw. Theory Techn.*, vol. 69, no. 3, pp. 1791–1804, Mar. 2021.

[17] J. Park, D.-H. Jung, and S.-O. Park, "Strategic method of determining parameter values in frequency modulated continuous wave radar for low noise floor over middle-long range," *Microw. Opt. Technol. Lett.*, vol. 63, no. 6, pp. 1727–1731, 2021.

[18] I. G. Cumming and F. H. Wong, *Digital Processing of Synthetic Aperture Radar Data: Algorithms and Implementation*. Norwood, MA, USA: Artech House, 2005.
[19] B.-L. Cho, Y.-K. Kong, H.-G. Park, and Y.-S. Kim, "Automobile-based SAR/InSAR system for ground experiments," *IEEE Geosci. Remote Sens. Lett.*, vol. 3, no. 3, pp. 401–405, Jul. 2006.
[20] D.-H. Jung, H.-S. Kang, C.-K. Kim, J. Park, and S.-O. Park, "Sparse scene recovery for high-resolution automobile FMCW SAR via scaled compressed sensing," *IEEE Trans. Geosci. Remote Sens.*, vol. 57, no. 12, pp. 10136–10146, Dec. 2019, doi: 10.1109/TGRS.2019.2931626.
[21] J. C. Curlander and R. N. McDonough, *Synthetic Aperture Radar Systems and Signal Processing*. New York, NY, USA: Wiley, 1991.
[22] A. V. Oppenheim and A. S. Willsky, *Signals and Systems*. Englewood Cliffs, NJ, USA: Prentice-Hall, 1983.
[23] D. M. Pozar, *Microwave Engineering*, 4th ed. Hoboken, NJ, USA: Wiley, 2012.
[24] B. Razavi, *RF Microelectronics*. Upper Saddle River, NJ, USA: Prentice-Hall, 2011.
[25] J. O. Smith III, *Spectral Audio Signal Processing*. New York, NY, USA: W3K Publishing, 2011.
[26] J. O. Smith III, *Center for Computer Research in Music and Acoustic (CCRMA)*. Stanford, CA, USA: Stanford Univ., 2009.
[27] M. Born and E. Wolf, *Principles of Optics*, 7th ed. Cambridge, U.K.: Cambridge Univ. Press, 1999.
[28] C. K. Kim, M. Y. Park, G. H. Shin, and S. O. Park, "An improved technique for single-channel video-SAR based on fractional Fourier transform," *IEEE Trans. Aerosp. Electron. Syst.*, vol. 58, no. 5, pp. 4044–4052, Oct. 2022, doi: 10.1109/TAES.2022.3157657.
[29] P. Kenneth and M. de Bernard, "Direct detection LiDAR system and method with synthetic Doppler processing," U.S. Patent 11 460 550 B2, Apr. 10, 2022.
[30] K. J. Yoo, "Signal processing device for radar device and object detection method," Korea Patent 0 048 169, Apr. 25, 2019.
[31] Y. Xining, S. J. Frederick, and L. Zhengzheng, "Object range and velocity detection from varying radar pulse repetition times," Europe Patent 3 796 038 A1, Mar. 24, 2021.
[32] J. E. Lee, "Radar device and method for detecting an object based on whether an event occurs," Korea Patent 0 184 951, Dec. 28, 2020.

Jun Sung Park was born in Daegu, South Korea, in 1993. He received the B.S. degree from Kyungpook National University, Daegu, South Korea, in 2017, and the M.S. degree in electrical engineering from the Korea Advanced Institute of Science and Technology, Daejeon, South Korea, in 2019, where he is currently pursuing the Ph.D. degree in electrical engineering.

His current research interests include radar systems and radar signal processing.

Chul Ki Kim was born in Gangneung, South Korea, in July 1989. He received the B.S. degree in electronic engineering from Soongsil University, Seoul, South Korea, in 2014, and the M.S. and Ph.D. degrees in electrical engineering from the Korea Advanced Institute of Science and Technology (KAIST), Daejeon, South Korea, in 2016 and 2021, respectively.

From 2016 to 2017, he was with the Satellite Technology Research Center (SaTRec), KAIST, where he finished the course of post-doctoral research at the Electric and Information Research Center, in 2021. He is currently with the Research and Development Research Center, HYUNDAI MOBIS, Gyeonggi, South Korea. His current research interests include advanced driver assistance radar systems (ADAS), radar hardware system design, synthetic aperture radar (SAR) signal processing, and electromagnetics theory.

Seong Ook Park (Senior Member, IEEE) was born in Kyungpook, South Korea, in December 1964. He received the B.S. degree in electrical engineering from Kyungpook National University, Daegu, South Korea, in 1987, the M.S. degree in electrical engineering from the Korea Advanced Institute of Science and Technology, Daejeon, South Korea, in 1989, and the Ph.D. degree in electrical engineering from Arizona State University, Tempe, AZ, USA, in 1997.

From March 1989 to August 1993, he was a Research Engineer with Korea Telecom, Daejeon, with a focus on the microwave systems and networks. He joined the Telecommunication Research Center, Arizona State University, until September 1997. Since October 1997, he has been with the Information and Communications University, Daejeon. He is currently a Professor with the Korea Advanced Institute of Science and Technology. His research interests include mobile handset antenna and analytical and numerical techniques in the area of electromagnetics.

Dr. Park is a member of Phi Kappa Phi.